
DPOK: Reinforcement Learning for Fine-tuning Text-to-Image Diffusion Models

Ying Fan^{*,1,2}, Olivia Watkins³, Yuqing Du³, Hao Liu³, Moonkyung Ryu¹, Craig Boutilier¹,
Pieter Abbeel³, Mohammad Ghavamzadeh¹, Kangwook Lee², Kimin Lee^{*,1}

^{*}Equal technical contribution

¹Google Research ²University of Wisconsin-Madison ³UC Berkeley

Abstract

Learning from human feedback has been shown to improve text-to-image models. These techniques first learn a reward function that captures what humans care about in the task and then improve the models based on the learned reward function. Even though relatively simple approaches (e.g., rejection sampling based on reward scores) have been investigated, fine-tuning text-to-image models with the reward function remains challenging. In this work, we propose using online reinforcement learning (RL) to fine-tune text-to-image models. We focus on *diffusion models*, defining the fine-tuning task as an RL problem, and updating the pre-trained text-to-image diffusion models using policy gradient to maximize the feedback-trained reward. Our approach, coined DPOK, integrates policy optimization with KL regularization. We conduct an analysis of KL regularization for both RL fine-tuning and supervised fine-tuning. In our experiments, we show that DPOK is generally superior to supervised fine-tuning with respect to both image-text alignment and image quality.

1 Introduction

Recent advances in *diffusion models* [10, 36, 37], together with pre-trained text encoders (e.g., CLIP [28], T5 [29]) have led to impressive results in text-to-image generation. Large-scale text-to-image models, such as Imagen [33], Dalle-2 [30] and Stable Diffusion [31], generate high-quality, creative images given novel text prompts. However, despite these advances, current models have systematic weaknesses. For example, current models have a limited ability to compose multiple objects [6, 7, 26]. They also frequently encounter difficulties when generating objects with specified colors and counts [12, 18].

Learning from human feedback (LHF) has proven to be an effective means to overcome these limitations [14, 18, 41, 43]. Lee et al. [18] demonstrate that certain properties, such as generating objects with specific colors, counts, and backgrounds, can be improved by learning a *reward function* from human feedback, followed by fine-tuning the text-to-image model using supervised learning. They show that simple supervised fine-tuning based on reward-weighted loss can improve the reward scores, leading to better image-text alignment. However, supervised fine-tuning often induces a deterioration in image quality (e.g., over-saturated or non-photorealistic images). This is likely due to the model being fine-tuned on a fixed dataset that is generated by a pre-trained model (Figure 1(a)).

In this work, we explore using *online reinforcement learning (RL)* for fine-tuning text-to-image diffusion models (Figure 1(b)). We show that optimizing the expected reward of a diffusion model’s image output is equivalent to performing policy gradient on a multi-step diffusion model under certain regularity assumptions. We also incorporate Kullback–Leibler (KL) divergence with respect to the pre-trained model as regularization in an online manner, treating this as an implicit reward.

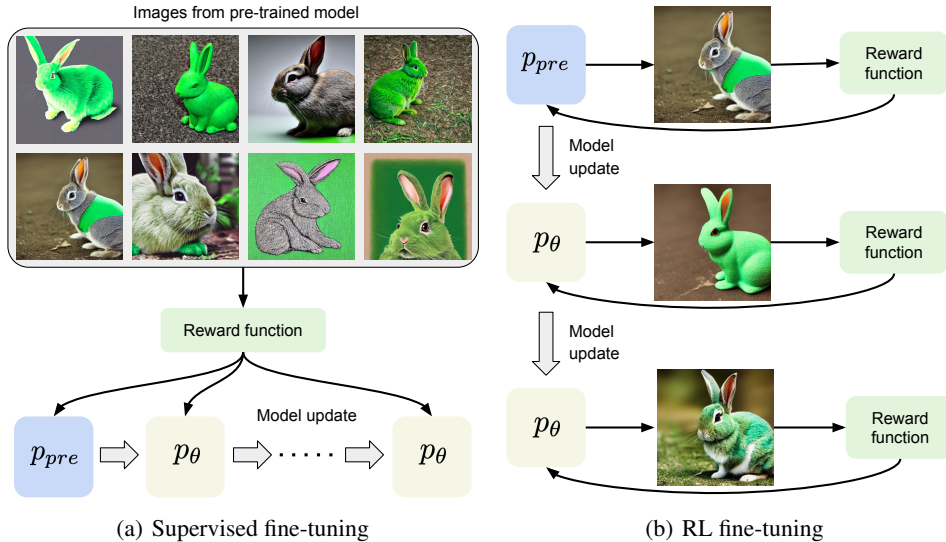


Figure 1: Illustration of (a) reward-weighted supervised fine-tuning and (b) RL fine-tuning. Both start with the same pre-trained model (the blue rectangle). In supervised fine-tuning, the model is updated on a fixed dataset generated by the pre-trained model. In contrast, the model is updated using new samples from the previously trained model during online RL fine-tuning.

In our experiments, we fine-tune the Stable Diffusion model [31] using ImageReward [43], an open-source reward model trained on a large dataset comprised of human assessments of (text, image) pairs. We show that online RL fine-tuning achieves strong text-image alignment while maintaining high image fidelity by optimizing its objective in an online manner. *Crucially, online training allows evaluation of the reward model and conditional KL divergence beyond the (supervised) training dataset.* This offers distinct advantages over supervised fine-tuning, a point we demonstrate empirically. In our empirical comparisons, we also incorporate the KL regularizer in a supervised fine-tuning method for a fair comparison.

Our contributions are as follows:

- We frame the optimization of the expected reward (w.r.t. an LHF-reward) of the image output from a diffusion model given text prompts as an online RL problem. Moreover, we present DPOK: **D**iffusion **P**olicy **O**ptimization with **K**L regularization, which utilizes KL regularization w.r.t. the pre-trained text-to-image model as an implicit reward to stabilize RL fine-tuning.
- We study incorporating KL regularization into supervised fine-tuning of diffusion models, which can mitigate some failure modes (e.g., generating over-saturated images) in [18]. This also allows a fairer comparison with our RL technique.
- We discuss key differences between supervised fine-tuning and online fine-tuning of text-to-image models (Section 4.3).
- Empirically, we show that online fine-tuning is effective in optimizing rewards, which improves text-to-image alignment while maintaining high image fidelity.

2 Related Work

Text-to-image diffusion models. Diffusion models [10, 36, 38] are a class of generative models that use an iterative denoising process to transform Gaussian noise into samples that follow a learned data distribution. These models have proven to be highly effective in a range of domains, including image generation [4], audio generation [15], 3D synthesis [27] and robotics [3]. When combined with large-scale language encoders [28, 29], diffusion models have demonstrated impressive performance in text-to-image generation [30, 31, 33]. However, there are still many known weaknesses of existing text-to-image models, such as compositionality and attribute binding [6, 21] or text rendering [22].

Learning from human feedback. Human assessments of (or preferences over) learned model outcomes have been used to guide learning on a variety of tasks, ranging from learning behaviors [17] to language modeling [1, 24, 20, 40]. Recent work has also applied such methods to improve the alignment of text-to-image models. Human preferences are typically gathered at scale by asking annotators to compare generations, and a *reward model* is trained (for example, by fine-tuning a vision-language model such as CLIP [28] or BLIP [19]) to produce scalar rewards well-aligned with the human data [43, 13]. The reward model is used to improve text-to-image model quality by fine-tuning a pre-trained generative model [18, 42]. Unlike prior approaches, which typically focus on reward-filtered or reward-weighted supervised learning, we develop an online fine-tuning framework with an RL-based objective.

RL fine-tuning of diffusion models. Fan & Lee [5] first introduce a method to improve pre-trained diffusion models by integrating policy gradient and GAN training [8]. They use policy gradient with reward signals from the discriminator to update the diffusion model and demonstrate that the fine-tuned model can generate realistic samples with few diffusion steps with DDPM sampling [10] on relatively simple domains (e.g., CIFAR [16] and CelebA [23]). In this work, we explore RL fine-tuning especially for large-scale text-to-image models using human rewards. We also consider several design choices like adding KL regularization as an implicit reward, and compare RL fine-tuning to supervised fine-tuning.

Concurrent and independent from our work, Black et al. [2] have also investigated RL fine-tuning to fine-tune text-to-image diffusion models. They similarly frame the fine-tuning problem as a multi-step decision-making problem, and demonstrate that RL fine-tuning can outperform supervised fine-tuning with reward-weighted loss [18] in optimizing the reward, which aligns with our own observations. Furthermore, our work analyzes KL regularization for both supervised fine-tuning and RL fine-tuning with theoretical justifications, and shows that adopting KL regularization is useful in addressing some failure modes (e.g., deterioration in image quality) of fine-tuned models. For a comprehensive discussion of prior work, we refer readers to Appendix D.

3 Problem Setting

In this section, we describe our basic problem setting for text-to-image generation of diffusion models.

Diffusion models. We consider the use of *denoising diffusion probabilistic models (DDPMs)* [10] for image generation and draw our notation and problem formulation from this paper. Let q_0 be the data distribution, i.e., $x_0 \sim q_0(x_0)$, $x_0 \in \mathbb{R}^n$. A DDPM approximates q_0 with a parameterized model of the form $p_\theta(x_0) = \int p_\theta(x_{0:T}) dx_{1:T}$. The *reverse process* is a Markov chain with the following dynamics:

$$p_T(x_T) = \mathcal{N}(0, I), \quad p_\theta(x_{t-1}|x_t) = \mathcal{N}(\mu_\theta(x_t, t), \Sigma_t). \quad (1)$$

And we have $p_\theta(x_{0:T}) = p_T(x_T) \prod_{t=1}^T p_\theta(x_{t-1}|x_t)$. A unique characteristic of DDPMs is the exploitation of an approximate posterior $q(x_{1:T}|x_0)$, known as the *forward* or *diffusion process*, which is itself a Markov chain that adds Gaussian noise to the data according to a variance schedule β_1, \dots, β_T :

$$q(x_{1:T}|x_0) = \prod_{t=1}^T q(x_t|x_{t-1}), \quad q(x_t|x_{t-1}) = \mathcal{N}(\sqrt{1-\beta_t} x_{t-1}, \beta_t I). \quad (2)$$

Let $\alpha_t = 1 - \beta_t$, $\bar{\alpha}_t = \prod_{s=1}^t \alpha_s$, and $\tilde{\beta}_t = \frac{1-\bar{\alpha}_{t-1}}{1-\bar{\alpha}_t} \beta_t$. Ho et al. [10] adopt the parameterization $\mu_\theta(x_t, t) = \frac{1}{\sqrt{\alpha_t}} \left(x_t - \frac{\beta_t}{\sqrt{1-\bar{\alpha}_t}} \epsilon_\theta(x_t, t) \right)$.

Training a DDPM is performed by optimizing a variational bound on the negative log-likelihood $\mathbb{E}[-\log p_\theta(x_0)]$, which is equivalent to optimizing:

$$\mathbb{E}_q \left[\sum_{t=1}^T \text{KL}(q(x_{t-1}|x_t, x_0) \| p_\theta(x_{t-1}|x_t)) \right]. \quad (3)$$

Note that the variance sequence $(\beta_t)_{t=1}^T \in (0, 1)^T$ is chosen such that $\bar{\alpha}_T \approx 0$, and thus, $q(x_T|x_0) \approx \mathcal{N}(0, I)$. The covariance matrix Σ_t in (1) is often set to either $\beta_t I$ or $\tilde{\beta}_t I$, which is not trainable. Unlike the original DDPM, we use a latent diffusion model [31], so x_t are latents.

Text-to-image diffusion models. Diffusion models are especially well-suited to *conditional* data generation, as required by text-to-image models: one can plug in a classifier as guidance function [4], or can directly train the diffusion model’s conditional distribution with classifier-free guidance [9].

Given text $z \sim p(z)$, let $q(x_0|z)$ be the conditional data distribution given the text prompt, which induces a joint distribution $p(x_0, z)$. During training, the same noising process q is used regardless of input z , and both the unconditional denoising model $\epsilon_\theta(x_t, t)$ and a conditional denoising model $\epsilon_\theta(x_t, t, z)$ are learned. For data sampling, let $\bar{\epsilon}_\theta = w\epsilon_\theta(x_t, t, z) + (1 - w)\epsilon_\theta(x_t, t)$, where $w \geq 1$ is the guidance scale. At test time, given a text prompt z , the model generates conditional data according to $p_\theta(x_0|z)$.

4 Fine-tuning of Diffusion Models

In this section, we detail our approach for online RL fine-tuning of diffusion models. We treat diffusion as an MDP, which allows us to optimize rewards using the RL policy gradient algorithm. Our approach also incorporates a KL term to ensure that the updated model is not too far from the original model. For comparison, we also present a modified supervised fine-tuning method with KL regularization, and discuss the difference between these two approaches.

4.1 RL Fine-tuning with KL Regularization

We first outline the primary approach. Let $p_\theta(x_{0:T}|z)$ be a text-to-image diffusion model where z is some text prompt distributed according to $p(z)$, and let $r(x_0, z)$ be a reward model (typically trained using human assessment of images). Our goal is to re-train/fine-tune the diffusion model to maximize the expected reward of the generated images given the prompt distribution, *i.e.*,

$$\min_{\theta} \mathbb{E}_{p(z)} \mathbb{E}_{p_\theta(x_0|z)} [-r(x_0, z)]. \quad (4)$$

We obtain the following gradient of this objective function:

Lemma 4.1 (A modification of Theorem 4.1 in [5]). *If $p_\theta(x_{0:T}|z)r(x_0, z)$ and $\nabla_\theta p_\theta(x_{0:T}|z)r(x_0, z)$ are continuous functions of θ , $x_{0:T}$, and z , then we can write the gradient of the objective in (4) as*

$$\nabla_\theta \mathbb{E}_{p(z)} \mathbb{E}_{p_\theta(x_0|z)} [-r(x_0, z)] = \mathbb{E}_{p(z)} \mathbb{E}_{p_\theta(x_{0:T}|z)} \left[-r(x_0, z) \sum_{t=1}^T \nabla_\theta \log p_\theta(x_{t-1}|x_t, z) \right]. \quad (5)$$

Proof. We present the proof in Appendix A.1. □

This equation becomes identical to the policy gradient equation if we treat the dynamics of the diffusion process as a Markov decision process (MDP). Specifically, the MDP has horizon T , one timestep for each diffusion step. We treat $p_\theta(x_{t-1}|x_t, z)$ as a *policy* given prompt z . We start in a sampled initial state x_T . Given x_t , the action at each timestep is $a = x_{t-1}$, and the next state given by the "environment" is identical to the action. The reward is $r(x_0, z)$ at the final step, and 0 at any other step. On this view, Eq. (5) is equivalent to performing policy gradient in the MDP. Note that we keep the covariance Σ_t as constant in DDPM and only train μ_θ , such that it would naturally provide a stochastic policy for online exploration.

Notice that this RL-based policy gradient approach is not the only way to optimize objective (5). Alternatively, one could compute the gradient through the trajectories to update the model; but the multi-step nature of diffusion models makes this approach memory inefficient and potentially prone to numerical instability. Consequently, scaling it to high-resolution images becomes challenging. For this reason, we adopt policy gradient to train large-scale diffusion models like Stable Diffusion [31].

KL regularization in an online manner. The risk of fine-tuning based purely on the LHF-generated reward model is that it may discount the "skill" of the initial diffusion model to a greater degree than warranted. To avoid overfitting the reward model, we incorporate the KL divergence between the fine-tuned model and the pre-trained model as a regularizer. We consider KL divergence between the current model and the pre-trained model as a regularization term similar to [24, 40].

Algorithm 1 DPOK: Diffusion policy optimization with KL regularization

Input: Reward model r , pre-trained diffusion model p_{pre} , diffusion model p_{θ} , sampling batch size m , training batch size n , reward weight α , KL weight β , text distribution $p(z)$

Initialize $p_{\theta} = p_{\text{pre}}$

while θ not converged **do**

Obtain m i.i.d. samples by first sampling $z \sim p(z)$ and then $x_{0:T} \sim p_{\theta}(x_{0:T}|z)$

Randomly select n transition samples, final output and text condition: $\{x_{t-1}, x_t, x_0, z\}$

Take gradient step on

$$\nabla_{\theta} \left(-\alpha r(x_0, z) \log p_{\theta}(x_{t-1}|x_t, z) + \beta \text{KL}(p_{\theta}(x_{t-1}|x_t, z) \| p_{\text{pre}}(x_{t-1}|x_t, z)) \right)$$

end while

Output: Fine-tuned diffusion model p_{θ}

Lemma 4.2. Assume that $p_{\text{pre}}(x_{0:T}|z)$ and $p_{\theta}(x_{0:T}|z)$ are both Markov chains starting from $x_T \sim \mathcal{N}(0, I)$ given text prompt z . Then we have

$$\mathbb{E}_{p(z)}[\text{KL}(p_{\theta}(x_0|z) \| p_{\text{pre}}(x_0|z))] \leq \mathbb{E}_{p(z)} \left[\sum_{t=1}^T \mathbb{E}_{p_{\theta}(x_t|z)}[\text{KL}(p_{\theta}(x_{t-1}|x_t, z) \| p_{\text{pre}}(x_{t-1}|x_t, z))] \right]. \quad (6)$$

See derivation in Appendix A.2. Intuitively, this lemma tells us that the divergence between the distributions of output images is upper-bounded by the sum of the divergences between the distributions over latents x_t at each diffusion step. Empirically, we use a combined objective function:

$$\mathbb{E}_{p(z)} \left[\alpha \mathbb{E}_{p_{\theta}^*(x_{0:T}|z)}[-r(x_0, z) \sum_{t=1}^T \log p_{\theta}(x_{t-1}|x_t, z)] + \beta \sum_{t=1}^T \mathbb{E}_{p_{\theta}^*(x_t|z)}[\text{KL}(p_{\theta}(x_{t-1}|x_t, z) \| p_{\text{pre}}(x_{t-1}|x_t, z))] \right]. \quad (7)$$

Here α, β are the reward weight and KL weight, respectively, and we use the notation p_{θ}^* to indicate that we treat it as constant when calculating the gradient. To see the difference between this KL regularization term and the upper bound in Lemma 4.2 (which does *not* treat p_{θ} as a constant when computing gradients), and why we use the latter one for experiments, please refer to Appendix A.3.

The full process of our framework, coined DPOK, is summarized in Algorithm 1.

4.2 Supervised Learning with KL Regularization

We now introduce KL regularization into supervised fine-tuning (SFT), which allows for a more meaningful comparison with our KL-regularized RL technique. We begin with a supervised fine-tuning objective similar to that used in [18]:

$$\mathbb{E}_{p(z)} \mathbb{E}_{p_{\text{pre}}(x_0|z)}[-r(x_0, z) \log p_{\theta}(x_0|z)]. \quad (8)$$

To compare with RL fine-tuning, we augment the supervised objective with a similar KL regularization term. Under the supervised learning setting, we consider $\text{KL}(p_{\text{pre}}(x_0|z) \| p_{\theta}(x_0|z))$, which is equivalent to minimizing $\mathbb{E}_{p_{\text{pre}}(x_0|z)}[-\log p_{\theta}(x_0|z)]$ given any z . Let $q(x_t)$ be the forward noising process used for training. Since the distribution of x_0 is generally not tractable, we use approximate upper bounds in the lemma below (see derivation in Appendix A.4):

Lemma 4.3. Let γ be the regularization weight. Assume $r(x_0, z) + \gamma > 0$ for all x_0, z . Let $f_{\theta}(x_t, t, z) := (x_t - \sqrt{1 - \alpha_t} \epsilon_{\theta}(x_t, t, z)) / \sqrt{\alpha_t}$, $\sigma_t^2 := \frac{1 - \alpha_t - 1}{1 - \alpha_t} \beta_t$. Then:

$$\begin{aligned} & \mathbb{E}_{p(z)} \mathbb{E}_{p_{\text{pre}}(x_0|z)}[-r(x_0, z) \log p_{\theta}(x_0|z)] + \gamma \mathbb{E}_{p(z)} \mathbb{E}_{p_{\text{pre}}(x_0|z)}[-\log p_{\theta}(x_0|z)] \\ & \leq \mathbb{E}_{p(z)} \mathbb{E}_{p_{\text{pre}}(x_0|z)} \left[(r(x_0, z) + \gamma) \sum_{t>1} \mathbb{E}_{q(x_t|x_0, z)} \left[\frac{\|x_0 - f_{\theta}(x_t, t, z)\|^2}{2\sigma_t^2} \right] \right] + C_1, \end{aligned} \quad (9)$$

Algorithm 2 Supervised fine-tuning with KL regularization

Input: Reward model r , pre-trained diffusion model p_{pre} , diffusion model p_{θ} , regularization weight γ , batch size n , the number of training samples M

Initialize $p_{\theta} = p_{\text{pre}}$

Collect M samples from pre-trained model: $\mathcal{D} = \{(x_0, z) \sim p_{\text{pre}}(x_0|z)p(z) | \forall i \in \{1, \dots, M\}\}$

while θ not converged **do**

 Obtain n i.i.d. samples $\{x_0, z\}$ from training dataset \mathcal{D}

 Sample x_t given $x_0, t \sim [1, T]$

 For KL-D, take gradient step on $\nabla_{\theta} \frac{(r(x_0, z) + \gamma) \|x_0 - f_{\theta}(x_t, t, z)\|^2}{2\sigma_t^2}$

 For KL-O, take gradient step on $\nabla_{\theta} \frac{r(x_0, z) \|x_0 - f_{\theta}(x_t, t, z)\|^2 + \gamma \|f_{\text{pre}}(x_t, t, z) - f_{\theta}(x_t, t, z)\|^2}{2\sigma_t^2}$

end while

Output: Fine-tuned diffusion model p_{θ}

Moreover, we also have another weaker upper bound:

$$\begin{aligned} & \mathbb{E}_{p(z)} \mathbb{E}_{p_{\text{pre}}(x_0|z)} [-r(x_0, z) \log p_{\theta}(x_0|z)] + \gamma \mathbb{E}_{p(z)} \mathbb{E}_{p_{\text{pre}}(x_0|z)} [-\log p_{\theta}(x_0|z)] \\ \leq & \mathbb{E}_{p(z)} \mathbb{E}_{p_{\text{pre}}(x_0|z)} \left[\sum_{t>1} \mathbb{E}_{q(x_t|x_0, z)} \left[\frac{r(x_0, z) \|x_0 - f_{\theta}(x_t, t, z)\|^2 + \gamma \|f_{\text{pre}}(x_t, t, z) - f_{\theta}(x_t, t, z)\|^2}{2\sigma_t^2} \right] \right] \\ & + C_2, \end{aligned} \tag{10}$$

where C_1 and C_2 are constants.

In Lemma 4.3, we introduce KL regularization (Eq. (9)) for supervised fine-tuning, which can be incorporated by adjusting the original reward with a shift factor γ in the reward-weighted loss, smoothing the weighting of each sample towards the uniform distribution.¹ We refer to this regularization as KL-D since it is based only on data from the pre-trained model. For KL-D, it induces the supervised training objective below:

$$\mathbb{E}_{p(z)} \mathbb{E}_{p_{\text{pre}}(x_0|z)} \left[(r(x_0, z) + \gamma) \sum_{t>1} \mathbb{E}_{q(x_t|x_0, z)} \left[\frac{\|x_0 - f_{\theta}(x_t, t, z)\|^2}{2\sigma_t^2} \right] \right]. \tag{11}$$

We also consider another KL regularization presented in Eq. (10). This KL regularization can be implemented by introducing an additional term in the reward-weighted loss. This extra term penalizes the L_2 distance between the denoising directions derived from the pre-trained model and the current model. We refer to it as KL-O because it also regularizes the output from the current model to be close to that from the pre-trained model. For KL-O, it induces the supervised training objective below:

$$\mathbb{E}_{p(z)} \mathbb{E}_{p_{\text{pre}}(x_0|z)} \left[\sum_{t>1} \mathbb{E}_{q(x_t|x_0, z)} \left[\frac{r(x_0, z) \|x_0 - f_{\theta}(x_t, t, z)\|^2 + \gamma \|f_{\text{pre}}(x_t, t, z) - f_{\theta}(x_t, t, z)\|^2}{2\sigma_t^2} \right] \right].$$

The full process of supervised fine-tuning is summarized in Algorithm 2. Note that our supervised setting requires only a pre-trained diffusion model and no extra/new datasets as a fair comparison to online RL training.

4.3 Contrasting Online RL Fine-tuning and Supervised Fine-tuning

We outline several key differences between online RL-based and supervised fine-tuning:

¹Intuitively, adjusting γ is similar to adjusting the temperature parameter in reward-weighted regression [25], a similar algorithm.

- **Online versus offline distribution.** We first contrast their objectives. The online RL objective is to find a new image distribution that maximizes expected reward—this can have much different support than the pre-trained distribution. In supervised fine-tuning, the objective only encourages the model to “imitate” good examples from the supervised dataset, which always lies in the support of the pre-trained distribution.
- **Different KL regularization.** The methods also differ in their use of KL regularization. The supervised KL regularizer considers upper bound of $\text{KL}(p_{\text{pre}}(x_0|z) \| p_{\theta}(x_0|z))$ while online KL regularizes upper bound of $\text{KL}(p_{\theta}(x_0|z) \| p_{\text{pre}}(x_0|z))$. More specifically, for online training, we evaluate conditional KL in each step using online samples, while for supervised training we evaluate conditional KL using supervised samples only. Moreover, online KL regularization can be seen as an extra reward function to encourage small divergence w.r.t. the pre-trained model for online optimization, while supervised KL induces an extra shift in the original reward for supervised training as shown in Lemma 4.3.
- **Different evaluation of the reward model.** Online RL fine-tuning evaluates the reward model using the updated distribution, while supervised fine-tuning evaluates the reward on the fixed pre-training data distribution. As a consequence, our online RL optimization should derive greater benefit from the generalization ability of the reward model.

For these reasons, we expect online RL fine-tuning and supervised fine-tuning to generate rather different behaviors. Specifically, online fine-tuning should be better at maximizing the combined reward (human reward and implicit KL reward) than the supervised approach (similar to the difference between online learning and weighted behavior cloning in reinforcement learning).

5 Experimental Evaluation

We now describe a set of experiments designed to test the efficacy of different fine-tuning methods.

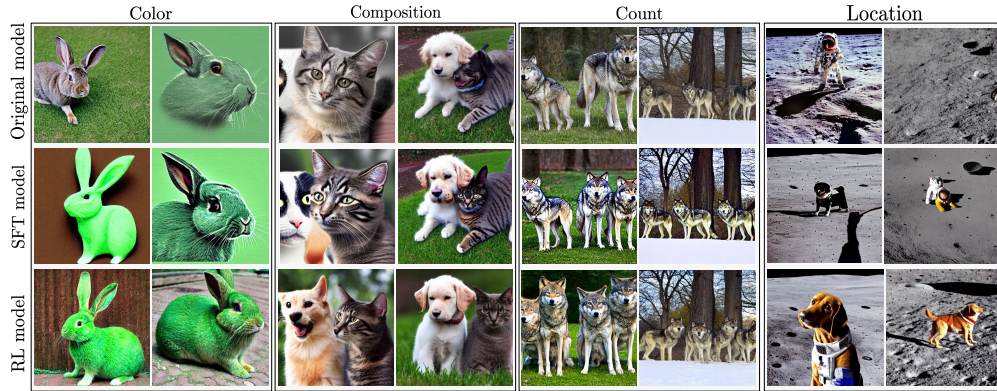
5.1 Experimental Setup

As our baseline generative model, we use Stable Diffusion v1.5 [31], which has been pre-trained on large image-text datasets [34, 35]. For compute-efficient fine-tuning, we use Low-Rank Adaption (LoRA) [11], which freezes the parameters of the pre-trained model and introduces low-rank trainable weights. We apply LoRA to the UNet [32] module and only update the added weights. For the reward model, we use ImageReward [43] which is trained on a large dataset comprised of human assessments of images. Compared to other scoring functions such as CLIP [28] or BLIP [19], ImageReward has a better correlation with human judgments, making it the preferred choice for fine-tuning our baseline diffusion model (see Appendix C for further justification). Further experimental details (e.g., model architectures, final hyper-parameters) are provided in Appendix B. We also provide more samples for qualitative comparison in Appendix E.4.

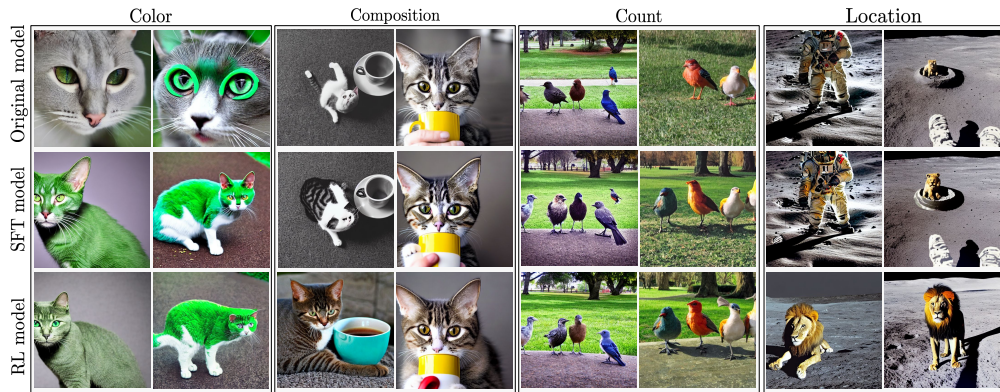
5.2 Comparison of Supervised and RL Fine-tuning

We first evaluate the performance of the original and fine-tuned text-to-image models w.r.t. specific capabilities, such as generating objects with specific colors, counts, or locations; and composing multiple objects (or *composition*). For both RL and SFT training we include KL regularization (see hyperparameters in Appendix B). For SFT, we adopt KL-O since we found it is more effective than KL-D in improving visual quality of the SFT model (see comparison between KL-O and KL-D in Section 5.3 and Section 5.3.2.). To systematically analyze the effects of different fine-tuning methods, we adopt a straightforward setup that uses one text prompt during fine-tuning. As training text prompts, we use “A green colored rabbit”, “A cat and a dog”, “Four wolves in the park”, and “A dog on the moon”. These test the models’ ability to handle prompts involving *color*, *composition*, *counting* and *location*, respectively. For supervised fine-tuning, we use 20K images generated by the original model, which is the same number of (online) images used by RL fine-tuning.

Figure 3(a) compares ImageReward scores of images generated by the different models (with the same random seed). We see that both SFT and RL fine-tuning improve the ImageReward scores on the training text prompt. This implies the fine-tuned models can generate images that are better aligned with the input text prompts than the original model because ImageReward is trained on



(a) Seen text prompt



(b) Unseen text prompt

Figure 2: Comparison of images generated by the original Stable Diffusion model, supervised fine-tuned (SFT) model, and RL fine-tuned model. Images in the same column are generated with the same random seed. (a) Images from seen text prompts: “A green colored rabbit” (color), “A cat and a dog” (composition), “Four wolves in the park” (count), and “A dog on the moon” (location). (b) Images from unseen text prompts: “A green colored cat” (color), “A cat and a cup” (composition), “Four birds in the park” (count), and “A lion on the moon” (location).

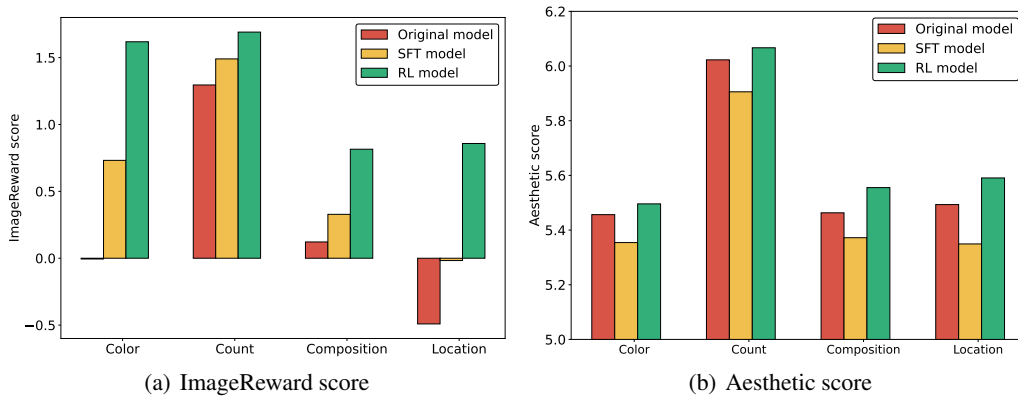


Figure 3: (a) ImageReward scores and (b) Aesthetic scores of three models: the original model, supervised fine-tuned (SFT) model, and RL fine-tuned model. ImageReward and Aesthetic scores are averaged over 50 samples from each model.

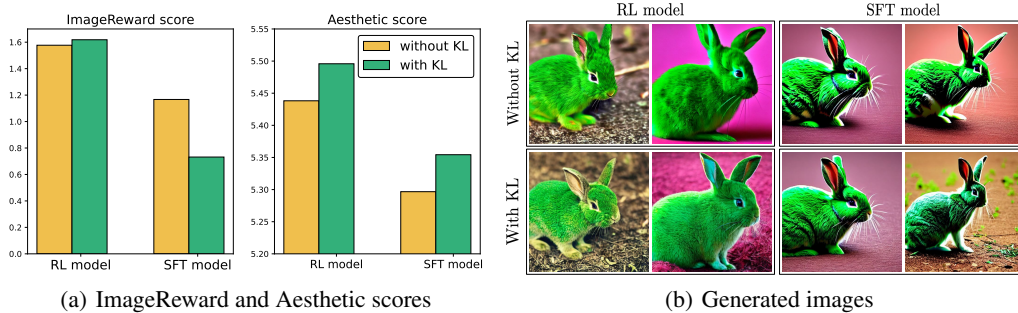


Figure 4: Ablation study of KL regularization in both SFT and RL training, trained on a single prompt “A green colored rabbit”. (a) ImageReward and Aesthetic scores are averaged over 50 samples from each model. (b) Images generated by RL models and SFT models optimized with and without KL regularization. Images in the same column are generated with the same random seed.

human feedback datasets to evaluate image-text alignment. Figure 2(a) indeed shows that fine-tuned models add objects to match the number (e.g., adding more wolves in “Four wolves in the park”), and replace incorrect objects with target objects (e.g., replacing an astronaut with a dog in “A dog on the moon”) compared to images from the original model. They also avoid obvious mistakes like generating a rabbit with a green background given the prompt “A green colored rabbit”. Of special note, we find that the fine-tuned models generate better images than the original model on several unseen text prompts consisting of unseen objects in terms of image-text alignment (see Figure 2(b)).

As we can observe in Figure 3(a), RL models enjoy higher ImageReward than SFT models when evaluated with the same training prompt in different categories respectively, due to the benefit of online training as we discuss in Section 4.3. We also evaluate the image quality of the three models using the aesthetic predictor [35], which is trained to predict the aesthetic aspects of generated images.² Figure 3(b) shows that supervised fine-tuning degrades image quality relative to the RL approach (and sometimes relative to the pre-trained model), even with KL regularization which is intended to blunt such effects. For example, the supervised model often generates over-saturated images, corroborating the observations of Lee et al. [18]. By contrast, the RL model generates more natural images that are at least as well-aligned with text prompts.

In this section, we focus on a single prompt training setup for systematic analysis of different fine-tuning approaches. For more complex setups, see Section 5.5 for training in the multi-prompt regime and Appendix E for examples of longer and more complex prompts.

5.3 The Effect of KL Regularization

5.3.1 Supervised KL Regularization vs Online KL Regularization

To demonstrate the impact of KL regularization on both supervised fine-tuning (SFT) and online RL fine-tuning, we conduct an ablation study specifically fine-tuning the pre-trained model with and without KL regularization on “A green colored rabbit”.

Figure 4(a) shows that KL regularization in online RL is effective in attaining both high reward and aesthetic scores. We observe that the RL model without KL regularization can generate lower-quality images (e.g., over-saturated colors and unnatural shapes) as shown in Figure 4(b). In the case of SFT with KL-O (where we use the same configuration as Section 5.2), we find that the KL regularization can mitigate some failure modes of SFT without KL and improve aesthetic scores, but generally suffers from lower ImageReward. We expect that this difference in the impact of KL regularization is due to the different nature of online and offline training—KL regularization is only applied to fixed samples in the case of SFT while KL regularization is applied to new samples per each update in the case of online RL (see Section 4.3 for related discussions).

²The aesthetic predictor had been utilized to filter out the low-quality images in training data for Stable Diffusion models.

5.3.2 KL-D vs KL-O: Ablation Study on Supervised KL Regularization

We also present the effects of both KL-D and KL-O with coefficient $\gamma \in \{0.1, 1.0, 2.0, 5.0\}$ in Figure 5 and Figure 6. We observe the followings:

- KL-D (eq. (9)) can slightly increase the aesthetic score. However, even with a large value of γ , it does not yield a significant improvement in visual quality. Moreover, it tends to result in lower ImageReward scores overall.
- In Figure 6, it is evident that KL-O is more noticeably effective in addressing the failure modes in supervised fine-tuning (SFT) compared to KL-D, especially when γ is relatively large. However, as a tradeoff, KL-O significantly reduces the ImageReward scores in that case.
- In general, achieving both high ImageReward and aesthetic scores simultaneously is challenging for supervised fine-tuning (SFT), unlike RL fine-tuning (blue bar in Figure 5).

We also present more qualitative examples from different choices of KL regularization in Appendix E.3.

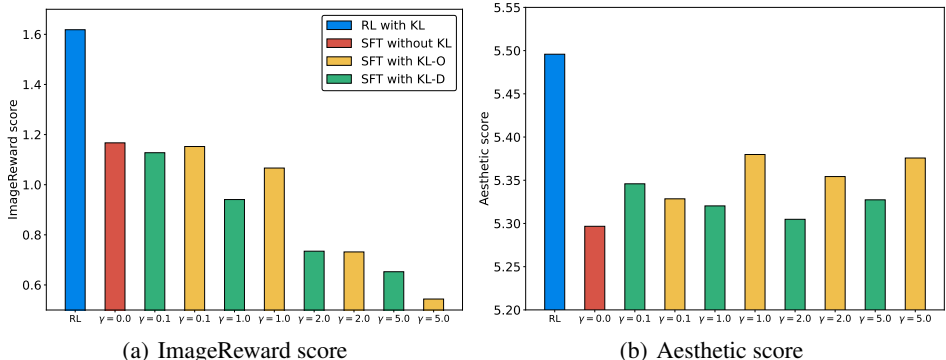


Figure 5: (a) ImageReward scores and (b) Aesthetic scores of supervised fine-tuned (SFT) models with different choices of regularization term and coefficient (γ) on text prompt "A green colored rabbit". Each score is averaged over 50 samples from each model. KL-O and KL-D refer to eq. (10) and eq. (9), respectively.

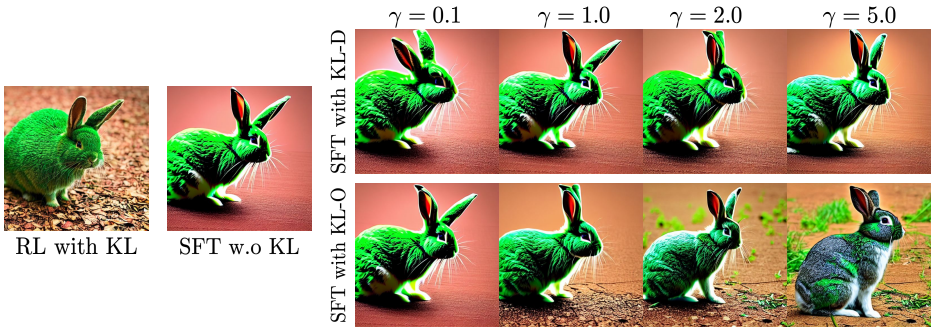


Figure 6: **(Left)** Sample from the RL model with KL regularization and sample from the SFT model without KL regularization. **(Right)** Samples from supervised fine-tuned models with different choices of regularization term and coefficient (γ) on "A green colored rabbit". As we increase γ in the SFT case, there is a tradeoff between alignment with the prompt and image quality (i.e. oversaturation). On the other hand, the RL with KL sample is able to retain both alignment and image quality.

5.4 Reducing Bias in the Pre-trained Model

To see the benefits of optimizing for ImageReward, we explore the effect of RL fine-tuning in reducing bias in the pre-trained model. Because the original Stable Diffusion model is trained on



Figure 7: Comparison of images generated by the original model and RL fine-tuned model on text prompt “Four roses”. The original model, which is trained on large-scale datasets from the web [35, 34], tends to produce whiskey-related images from “Four roses” due to the existence of a whiskey brand bearing the same name as the prompt. In contrast, RL fine-tuned model with ImageReward generates images associated with the flower “rose”.

	Original model	SFT model		RL model	
		Single	Multi	Single	Multi
ImageReward score	0.23	0.63	0.55	1.25	1.10
Aesthetic score	5.61	5.50	5.49	5.68	5.70

Table 1: ImageReward scores and Aesthetic scores from the original model, supervised fine-tuned (SFT) model, and RL fine-tuned model, all are trained on four text prompts simultaneously. We report the average ImageReward and Aesthetic scores across 200 images (50 images per each prompt). For SFT and RL models, we also provide the average performance of fine-tuned models trained on single prompts (Single) for comparison. All SFT models are trained with KL-O regularization as in Section 5.2.

large-scale datasets extracted from the web [34, 35], it can encode some biases in the training data. As shown in Figure 7, we see that the original model tends to produce whiskey-related images given the prompt “Four roses” (which happens to be the brand name of a whiskey), which is not aligned with users’ intention in general. To verify whether maximizing a reward model derived from human feedback can mitigate this issue, we fine-tune the original model on the “Four roses” prompt using RL fine-tuning. Figure 7 shows that the fine-tuned model generates images with roses (the flower) because the ImageReward score is low on the biased images (ImageReward score is increased to 1.12 from -0.52 after fine-tuning). This shows the clear benefits of learning from human feedback to better align existing text-to-image models with human intentions.

5.5 Fine-tuning on Multiple Prompts

We further verify the effectiveness of the proposed techniques for fine-tuning text-to-image models on multiple prompts simultaneously. We use four text prompts (i.e., “A green colored rabbit”, “A cat and a dog”, “Four wolves in the park”, and “A dog on the moon”), which are used in Section 5.2. For evaluation, we report the average ImageReward and Aesthetic scores across 200 images (50 images per each prompt). Table 1 shows that RL fine-tuning is more effective than SFT in improving both ImageReward and aesthetic scores across multiple prompts. However, we find that the ImageReward score of fine-tuned model on multiple prompts (Multi) is a bit lower than the average score of fine-tuned models on a single prompt (Single). We expect that this is due to the varying difficulty of each text prompt, which can pose additional challenges such as gradient conflict as observed in multi-task RL. We defer further investigation of fine-tuning on multiple prompts to future work.

6 Discussions

In this work, we propose DPOK, an algorithm to fine-tune a text-to-image diffusion model using policy gradient with KL regularization. We show that online RL fine-tuning outperforms simple supervised fine-tuning in improving the model’s performance. Also, we conduct an analysis of KL regularization for both methods and discuss the key differences between RL fine-tuning and

supervised fine-tuning. We believe our work demonstrates the potential of *reinforcement learning from human feedback* in improving text-to-image diffusion models.

Limitations, future directions. Several limitations of our work suggest interesting future directions: (a) As discussed in Section 5.5, fine-tuning on multiple prompts requires longer training time, hyperparameter tuning, and engineering efforts. More efficient training with a broader range of diverse and complex prompts would be an interesting future direction to explore. (b) Exploring advanced policy gradient methods can be useful for further performance improvement. Investigating the applicability and benefits of these methods could lead to improvements in the fine-tuning process.

Broader Impacts Text-to-image models can offer societal benefits across fields such as art and entertainment, but they also carry the potential for misuse. Our research allows users to finetune these models towards arbitrary reward functions. This process can be socially beneficial or harmful depending on the reward function used. Users could train models to produce less biased or offensive imagery, but they could also train them to produce misinformation or deep fakes. Since many users may follow our approach of using open-sourced reward functions for this finetuning, it is critical that the biases and failure modes of publicly available reward models are thoroughly documented.

Acknowledgements

We thank Deepak Ramachandran and Jason Baldrige for providing helpful comments and suggestions. OW and YD are funded by the Center for Human Compatible Artificial Intelligence.

References

- [1] Bai, Yuntao, Jones, Andy, Ndousse, Kamal, Askell, Amanda, Chen, Anna, DasSarma, Nova, Drain, Dawn, Fort, Stanislav, Ganguli, Deep, Henighan, Tom, et al. Training a helpful and harmless assistant with reinforcement learning from human feedback. *arXiv preprint arXiv:2204.05862*, 2022. 3
- [2] Black, Kevin, Janner, Michael, Du, Yilun, Kostrikov, Ilya, and Levine, Sergey. Training diffusion models with reinforcement learning. *arXiv preprint arXiv:2305.13301*, 2023. 3, 18
- [3] Chi, Cheng, Feng, Siyuan, Du, Yilun, Xu, Zhenjia, Cousineau, Eric, Burchfiel, Benjamin, and Song, Shuran. Diffusion policy: Visuomotor policy learning via action diffusion. *arXiv preprint arXiv:2303.04137*, 2023. 2
- [4] Dhariwal, Prafulla and Nichol, Alexander. Diffusion models beat gans on image synthesis. In *Advances in Neural Information Processing Systems*, 2021. 2, 4
- [5] Fan, Ying and Lee, Kangwook. Optimizing ddpm sampling with shortcut fine-tuning. *arXiv preprint arXiv:2301.13362*, 2023. 3, 4
- [6] Feng, Weixi, He, Xuehai, Fu, Tsu-Jui, Jampani, Varun, Akula, Arjun, Narayana, Pradyumna, Basu, Sugato, Wang, Xin Eric, and Wang, William Yang. Training-free structured diffusion guidance for compositional text-to-image synthesis. *arXiv preprint arXiv:2212.05032*, 2022. 1, 2
- [7] Gokhale, Tejas, Palangi, Hamid, Nushi, Besmira, Vineet, Vibhav, Horvitz, Eric, Kamar, Ece, Baral, Chitta, and Yang, Yezhou. Benchmarking spatial relationships in text-to-image generation. *arXiv preprint arXiv:2212.10015*, 2022. 1
- [8] Goodfellow, Ian, Pouget-Abadie, Jean, Mirza, Mehdi, Xu, Bing, Warde-Farley, David, Ozair, Sherjil, Courville, Aaron, and Bengio, Yoshua. Generative adversarial networks. *Communications of the ACM*, 63(11):139–144, 2020. 3
- [9] Ho, Jonathan and Salimans, Tim. Classifier-free diffusion guidance. *arXiv preprint arXiv:2207.12598*, 2022. 4
- [10] Ho, Jonathan, Jain, Ajay, and Abbeel, Pieter. Denoising diffusion probabilistic models. In *Advances in Neural Information Processing Systems*, 2020. 1, 2, 3, 16, 17

- [11] Hu, Edward J, Shen, Yelong, Wallis, Phillip, Allen-Zhu, Zeyuan, Li, Yuanzhi, Wang, Shean, Wang, Lu, and Chen, Weizhu. Lora: Low-rank adaptation of large language models. *arXiv preprint arXiv:2106.09685*, 2021. 7
- [12] Hu, Yushi, Liu, Benlin, Kasai, Jungo, Wang, Yizhong, Ostendorf, Mari, Krishna, Ranjay, and Smith, Noah A. Tifa: Accurate and interpretable text-to-image faithfulness evaluation with question answering. *arXiv preprint arXiv:2303.11897*, 2023. 1
- [13] Kirstain, Yuval, Polyak, Adam, Singer, Uriel, Matiana, Shahbuland, Penna, Joe, and Levy, Omer. Pick-a-pic: An open dataset of user preferences for text-to-image generation. *arXiv preprint arXiv:2305.01569*, 2023. 3
- [14] Kirstain, Yuval, Polyak, Adam, Singer, Uriel, Matiana, Shahbuland, Penna, Joe, and Levy, Omer. Pick-a-pic: An open dataset of user preferences for text-to-image generation. *arXiv preprint arXiv:2305.01569*, 2023. 1
- [15] Kong, Zhifeng, Ping, Wei, Huang, Jiaji, Zhao, Kexin, and Catanzaro, Bryan. Diffwave: A versatile diffusion model for audio synthesis. *arXiv preprint arXiv:2009.09761*, 2020. 2
- [16] Krizhevsky, Alex, Hinton, Geoffrey, et al. Learning multiple layers of features from tiny images. 2009. 3
- [17] Lee, Kimin, Smith, Laura, and Abbeel, Pieter. Pebble: Feedback-efficient interactive reinforcement learning via relabeling experience and unsupervised pre-training. *arXiv preprint arXiv:2106.05091*, 2021. 3
- [18] Lee, Kimin, Liu, Hao, Ryu, Moonkyung, Watkins, Olivia, Du, Yuqing, Boutilier, Craig, Abbeel, Pieter, Ghavamzadeh, Mohammad, and Gu, Shixiang Shane. Aligning text-to-image models using human feedback. *arXiv preprint arXiv:2302.12192*, 2023. 1, 2, 3, 5, 9, 18
- [19] Li, Junnan, Li, Dongxu, Xiong, Caiming, and Hoi, Steven. Blip: Bootstrapping language-image pre-training for unified vision-language understanding and generation. In *International Conference on Machine Learning*, 2022. 3, 7, 18
- [20] Liu, Hao, Sferrazza, Carmelo, and Abbeel, Pieter. Chain of hindsight aligns language models with feedback. *arXiv preprint arXiv:2302.02676*, 2023. 3
- [21] Liu, Nan, Li, Shuang, Du, Yilun, Torralba, Antonio, and Tenenbaum, Joshua B. Compositional visual generation with composable diffusion models. In *European Conference on Computer Vision*, 2022. 2
- [22] Liu, Rosanne, Garrette, Dan, Saharia, Chitwan, Chan, William, Roberts, Adam, Narang, Sharan, Blok, Irina, Mical, RJ, Norouzi, Mohammad, and Constant, Noah. Character-aware models improve visual text rendering. *arXiv preprint arXiv:2212.10562*, 2022. 2
- [23] Liu, Ziwei, Luo, Ping, Wang, Xiaogang, and Tang, Xiaoou. Deep learning face attributes in the wild. In *International Conference on Computer Vision*, 2015. 3
- [24] Ouyang, Long, Wu, Jeffrey, Jiang, Xu, Almeida, Diogo, Wainwright, Carroll, Mishkin, Pamela, Zhang, Chong, Agarwal, Sandhini, Slama, Katarina, Ray, Alex, et al. Training language models to follow instructions with human feedback. In *Advances in Neural Information Processing Systems*, 2022. 3, 4
- [25] Peters, Jan and Schaal, Stefan. Reinforcement learning by reward-weighted regression for operational space control. In *Proceedings of the 24th international conference on Machine learning*, pp. 745–750, 2007. 6
- [26] Petsiuk, Vitali, Siemenn, Alexander E, Surbehera, Saisamrit, Chin, Zad, Tyser, Keith, Hunter, Gregory, Raghavan, Arvind, Hicke, Yann, Plummer, Bryan A, Kerret, Ori, et al. Human evaluation of text-to-image models on a multi-task benchmark. *arXiv preprint arXiv:2211.12112*, 2022. 1
- [27] Poole, Ben, Jain, Ajay, Barron, Jonathan T, and Mildenhall, Ben. Dreamfusion: Text-to-3d using 2d diffusion. *arXiv preprint arXiv:2209.14988*, 2022. 2

- [28] Radford, Alec, Kim, Jong Wook, Hallacy, Chris, Ramesh, Aditya, Goh, Gabriel, Agarwal, Sandhini, Sastry, Girish, Askell, Amanda, Mishkin, Pamela, Clark, Jack, et al. Learning transferable visual models from natural language supervision. In *International Conference on Machine Learning*, 2021. [1](#), [2](#), [3](#), [7](#), [18](#)
- [29] Raffel, Colin, Shazeer, Noam, Roberts, Adam, Lee, Katherine, Narang, Sharan, Matena, Michael, Zhou, Yanqi, Li, Wei, and Liu, Peter J. Exploring the limits of transfer learning with a unified text-to-text transformer. *The Journal of Machine Learning Research*, 21(1):5485–5551, 2020. [1](#), [2](#)
- [30] Ramesh, Aditya, Dhariwal, Prafulla, Nichol, Alex, Chu, Casey, and Chen, Mark. Hierarchical text-conditional image generation with clip latents. *arXiv preprint arXiv:2204.06125*, 2022. [1](#), [2](#)
- [31] Rombach, Robin, Blattmann, Andreas, Lorenz, Dominik, Esser, Patrick, and Ommer, Björn. High-resolution image synthesis with latent diffusion models. In *Conference on Computer Vision and Pattern Recognition*, 2022. [1](#), [2](#), [3](#), [4](#), [7](#)
- [32] Ronneberger, Olaf, Fischer, Philipp, and Brox, Thomas. U-net: Convolutional networks for biomedical image segmentation. In *International Conference on Medical Image Computing and Computer Assisted Intervention*, 2015. [7](#)
- [33] Saharia, Chitwan, Chan, William, Saxena, Saurabh, Li, Lala, Whang, Jay, Denton, Emily, Ghasemipour, Seyed Kamyar Seyed, Ayan, Burcu Karagol, Mahdavi, S Sara, Lopes, Rapha Gontijo, et al. Photorealistic text-to-image diffusion models with deep language understanding. In *Advances in Neural Information Processing Systems*, 2022. [1](#), [2](#)
- [34] Schuhmann, Christoph, Vencu, Richard, Beaumont, Romain, Kaczmarczyk, Robert, Mullis, Clayton, Katta, Aarush, Coombes, Theo, Jitsev, Jenia, and Komatsuzaki, Aran. Laion-400m: Open dataset of clip-filtered 400 million image-text pairs. *arXiv preprint arXiv:2111.02114*, 2021. [7](#), [11](#)
- [35] Schuhmann, Christoph, Beaumont, Romain, Vencu, Richard, Gordon, Cade, Wightman, Ross, Cherti, Mehdi, Coombes, Theo, Katta, Aarush, Mullis, Clayton, Wortsman, Mitchell, et al. Laion-5b: An open large-scale dataset for training next generation image-text models. *arXiv preprint arXiv:2210.08402*, 2022. [7](#), [9](#), [11](#)
- [36] Sohl-Dickstein, Jascha, Weiss, Eric, Maheswaranathan, Niru, and Ganguli, Surya. Deep unsupervised learning using nonequilibrium thermodynamics. In *International Conference on Machine Learning*, 2015. [1](#), [2](#)
- [37] Song, Jiaming, Meng, Chenlin, and Ermon, Stefano. Denoising diffusion implicit models. *arXiv preprint arXiv:2010.02502*, 2020. [1](#)
- [38] Song, Yang and Ermon, Stefano. Improved techniques for training score-based generative models. In *Advances in neural information processing systems*, 2020. [2](#)
- [39] Song, Yang, Durkan, Conor, Murray, Iain, and Ermon, Stefano. Maximum likelihood training of score-based diffusion models. *Advances in Neural Information Processing Systems*, 34: 1415–1428, 2021. [15](#)
- [40] Stiennon, Nisan, Ouyang, Long, Wu, Jeffrey, Ziegler, Daniel, Lowe, Ryan, Voss, Chelsea, Radford, Alec, Amodei, Dario, and Christiano, Paul F. Learning to summarize with human feedback. *Advances in Neural Information Processing Systems*, 33:3008–3021, 2020. [3](#), [4](#)
- [41] Wu, Xiaoshi, Sun, Keqiang, Zhu, Feng, Zhao, Rui, and Li, Hongsheng. Better aligning text-to-image models with human preference. *arXiv preprint arXiv:2303.14420*, 2023. [1](#)
- [42] Wu, Xiaoshi, Sun, Keqiang, Zhu, Feng, Zhao, Rui, and Li, Hongsheng. Better aligning text-to-image models with human preference. *arXiv preprint arXiv:2303.14420*, 2023. [3](#)
- [43] Xu, Jiazheng, Liu, Xiao, Wu, Yuchen, Tong, Yuxuan, Li, Qinkai, Ding, Ming, Tang, Jie, and Dong, Yuxiao. Imagereward: Learning and evaluating human preferences for text-to-image generation. *arXiv preprint arXiv:2304.05977*, 2023. [1](#), [2](#), [3](#), [7](#), [18](#)

Appendix:

Reinforcement Learning for Fine-tuning Text-to-Image Diffusion Models

A Derivations

A.1 Lemma 4.1

Proof.

$$\begin{aligned}
& \nabla_{\theta} \mathbb{E}_{p(z)} \mathbb{E}_{p_{\theta}(x_0|z)} [-r(x_0, z)] = -\mathbb{E}_{p(z)} \left[\nabla_{\theta} \int p_{\theta}(x_0|z) r(x_0, z) dx_0 \right] \\
& = -\mathbb{E}_{p(z)} \left[\nabla_{\theta} \int \left(\int p_{\theta}(x_{0:T}|z) dx_{1:T} \right) r(x_0, z) dx_0 \right] \\
& = -\mathbb{E}_{p(z)} \left[\int \nabla_{\theta} \log p_{\theta}(x_{0:T}|z) \times r(x_0, z) \times p_{\theta}(x_{0:T}|z) dx_{0:T} \right] \\
& = -\mathbb{E}_{p(z)} \left[\int \nabla_{\theta} \log \left(p_T(x_T|z) \prod_{t=1}^T p_{\theta}(x_{t-1}|x_t, z) \right) \times r(x_0, z) \times p_{\theta}(x_{0:T}|z) dx_{0:T} \right] \\
& = -\mathbb{E}_{p(z)} \mathbb{E}_{p_{\theta}(x_{0:T}|z)} \left[r(x_0, z) \sum_{t=1}^T \nabla_{\theta} \log p_{\theta}(x_{t-1}|x_t, z) \right],
\end{aligned}$$

where the second to last equality is from the continuous assumptions of $p_{\theta}(x_{0:T}|z)r(x_0, z)$ and $\nabla_{\theta} p_{\theta}(x_{0:T}|z)r(x_0, z)$. \square

A.2 Lemma 4.2

Similar to the proof in Theorem 1 in [39], from data processing inequality with the Markov kernel, given any z we have

$$\text{KL}(p_{\theta}(x_0|z) \| p_{\text{pre}}(x_0|z)) \leq \text{KL}(p_{\theta}(x_{0:T}|z) \| p_{\text{pre}}(x_{0:T}|z)). \quad (12)$$

Using the Markov property of p_{θ} and p_{pre} , we have

$$\begin{aligned}
& \text{KL}(p_{\theta}(x_{0:T}|z) \| p_{\text{pre}}(x_{0:T}|z)) = \int p_{\theta}(x_{0:T}|z) \times \log \frac{p_{\theta}(x_{0:T}|z)}{p_{\text{pre}}(x_{0:T}|z)} dx_{0:T} \\
& = \int p_{\theta}(x_{0:T}|z) \log \frac{p_{\theta}(x_T|z) \prod_{t=1}^T p_{\theta}(x_{t-1}|x_t, z)}{p_{\text{pre}}(x_T|z) \prod_{t=1}^T p_{\text{pre}}(x_{t-1}|x_t, z)} dx_{0:T} \\
& = \int p_{\theta}(x_{0:T}|z) \left(\log \frac{p_{\theta}(x_T|z)}{p_{\text{pre}}(x_T|z)} + \sum_{t=1}^T \log \frac{p_{\theta}(x_{t-1}|x_t, z)}{p_{\text{pre}}(x_{t-1}|x_t, z)} \right) dx_{0:T} \\
& = \mathbb{E}_{p_{\theta}(x_{0:T}|z)} \left[\sum_{t=1}^T \log \frac{p_{\theta}(x_{t-1}|x_t, z)}{p_{\text{pre}}(x_{t-1}|x_t, z)} \right] = \sum_{t=1}^T \mathbb{E}_{p_{\theta}(x_{t:T}|z)} \mathbb{E}_{p_{\theta}(x_{0:t-1}|x_{t:T}, z)} \left[\log \frac{p_{\theta}(x_{t-1}|x_t, z)}{p_{\text{pre}}(x_{t-1}|x_t, z)} \right] \\
& = \sum_{t=1}^T \mathbb{E}_{p_{\theta}(x_t|z)} \mathbb{E}_{p_{\theta}(x_{0:t-1}|x_t, z)} \left[\log \frac{p_{\theta}(x_{t-1}|x_t, z)}{p_{\text{pre}}(x_{t-1}|x_t, z)} \right] = \sum_{t=1}^T \mathbb{E}_{p_{\theta}(x_t|z)} \mathbb{E}_{p_{\theta}(x_{t-1}|x_t, z)} \left[\log \frac{p_{\theta}(x_{t-1}|x_t, z)}{p_{\text{pre}}(x_{t-1}|x_t, z)} \right] \\
& = \sum_{t=1}^T \mathbb{E}_{p_{\theta}(x_t|z)} [\text{KL}(p_{\theta}(x_{t-1}|x_t, z) \| p_{\text{pre}}(x_{t-1}|x_t, z))].
\end{aligned}$$

Taking the expectation of $p(z)$ on both sides, we have

$$\mathbb{E}_{p(z)}[\mathbf{KL}(p_\theta(x_0|z))\|p_{\text{pre}}(x_0|z))] \leq \mathbb{E}_{p(z)} \left[\sum_{t=1}^T \mathbb{E}_{p_\theta(x_t|z)}[\mathbf{KL}(p_\theta(x_{t-1}|x_t, z)\|p_{\text{pre}}(x_{t-1}|x_t, z))] \right]. \quad (13)$$

A.3 The objective in Eq. (7)

From Lemma 4.2, for online fine-tuning, at each step $t \leq T$, we need to regularize $\sum_{t=1}^T \mathbb{E}_{p_\theta(x_t)}[\mathbf{KL}(p_\theta(x_{t-1}|x_t, z)\|p_{\text{pre}}(x_{t-1}|x_t, z))]$. By the product rule, we have

$$\begin{aligned} & \sum_{t=1}^T \nabla_\theta \mathbb{E}_{p_\theta(x_t)}[\mathbf{KL}(p_\theta(x_{t-1}|x_t, z)\|p_{\text{pre}}(x_{t-1}|x_t, z))] \\ &= \sum_{t=1}^T \mathbb{E}_{p_\theta(x_t)}[\nabla_\theta \mathbf{KL}(p_\theta(x_{t-1}|x_t, z)\|p_{\text{pre}}(x_{t-1}|x_t, z))] \\ &+ \sum_{t=1}^T \mathbb{E}_{p_\theta(x_t)}[\nabla_\theta \log p_\theta(x_t) \cdot \mathbf{KL}(p_\theta(x_{t-1}|x_t, z)\|p_{\text{pre}}(x_{t-1}|x_t, z))]. \end{aligned} \quad (14)$$

Moreover, the second term in Eq. (14) can be rewritten as

$$\begin{aligned} & \sum_{t=1}^T \mathbb{E}_{p_\theta(x_t)}[\nabla_\theta \log p_\theta(x_t) \cdot \mathbf{KL}(p_\theta(x_{t-1}|x_t, z)\|p_{\text{pre}}(x_{t-1}|x_t, z))] \\ &= \sum_{t=1}^T \mathbb{E}_{p_\theta(x_t)} \left[\sum_{t'>t}^T \nabla_\theta \log p_\theta(x_{t'-1}|x_{t'}, z) \cdot \mathbf{KL}(p_\theta(x_{t-1}|x_t, z)\|p_{\text{pre}}(x_{t-1}|x_t, z)) \right], \end{aligned} \quad (15)$$

which treats the sum of conditional KL-divergences along the prior sub-trajectory as a scalar reward at each step. However, computing these sums is more inefficient than just the first term in Eq. (14). Empirically, we find that regularizing only the first term in Eq. (14) works well, so we adopt this approach for simplicity, which yields the KL-regularized objective in Eq. (7).

A.4 Lemma 4.3

Similar to derivation in [10], and notice that q is not dependent on z (i.e., $q(\cdot \dots | z) = q(\cdot \dots)$), we have

$$\begin{aligned} & \mathbb{E}_{p(z)} \mathbb{E}_{p_{\text{pre}}(x_0|z)}[-(r(x_0, z) + \gamma) \log p_\theta(x_0|z)] \\ & \leq \mathbb{E}_{p(z)} \mathbb{E}_{p_{\text{pre}}(x_0|z)} \mathbb{E}_{q(x_{1:T}|x_0, z)} \left[-(r(x_0, z) + \gamma) \log \frac{p_\theta(x_{0:T}|z)}{q(x_{1:T}|x_0, z)} \right] \\ & = \mathbb{E}_{p(z)} \mathbb{E}_{p_{\text{pre}}(x_0|z)} \mathbb{E}_{q(x_{1:T}|x_0, z)} \left[-(r(x_0, z) + \gamma) \log \frac{p(x_T|z)}{q(x_T|x_0, z)} \right. \\ & \quad \left. - \sum_{t>1} (r(x_0, z) + \gamma) \log \frac{p_\theta(x_{t-1}|x_t, z)}{q(x_{t-1}|x_t, x_0, z)} \right] \\ & \quad - (r(x_0, z) + \gamma) \log p_\theta(x_0|x_1, z) \\ & = \mathbb{E}_{p(z)} \mathbb{E}_{p_{\text{pre}}(x_0|z)} \left[(r(x_0, z) + \gamma) \mathbb{E}_{q(x_T|x_0, z)}[\mathbf{KL}(q(x_T|x_0)\|p(x_T))] \right. \\ & \quad \left. + (r(x_0, z) + \gamma) \sum_{t>1} \mathbb{E}_{q(x_t|x_0, z)}[\mathbf{KL}(q(x_{t-1}|x_t, x_0)\|p_\theta(x_{t-1}|x_t, z))] \right. \\ & \quad \left. - (r(x_0, z) + \gamma) \mathbb{E}_{q(x_1|x_0, z)}[\log p_\theta(x_0|x_1, z)] \right], \end{aligned} \quad (16)$$

where the first inequality comes from ELBO. Let $f_\theta(x_t, t, z) := (x_t - \sqrt{1 - \alpha_t} \epsilon_\theta(x_t, t, z)) / \sqrt{\alpha_t}$, $\sigma_t^2 := \frac{1 - \bar{\alpha}_t - 1}{1 - \bar{\alpha}_t} \beta_t$. Optimizing the above bound is equivalent to optimizing

$$\begin{aligned} & \mathbb{E}_{p(z)} \mathbb{E}_{p_{\text{pre}}(x_0|z)} [(r(x_0, z) + \gamma) \mathbb{E}_{q(x_T|x_0, z)} [\text{KL}(q(x_T|x_0) \| p(x_T))] \\ & + (r(x_0, z) + \gamma) \sum_{t>1} \mathbb{E}_{q(x_t|x_0, z)} \left[\frac{\|x_0 - f_\theta(x_t, t, z)\|^2}{2\sigma_t^2} \right] \\ & - (r(x_0, z) + \gamma) \mathbb{E}_{q(x_1|x_0, z)} [\log p_\theta(x_0|x_1, z)]. \end{aligned} \quad (17)$$

Further more, from triangle inequality we have

$$\begin{aligned} & \sum_{t>1} \mathbb{E}_{q(x_t|x_0, z)} \left[\gamma \frac{\|x_0 - f_\theta(x_t, t, z)\|^2}{2\sigma_t^2} \right] \\ & \leq \sum_{t>1} \mathbb{E}_{q(x_t|x_0, z)} \left[\gamma \frac{\|x_0 - f_{\text{pre}}(x_t, t, z)\|^2 + \|f_{\text{pre}}(x_t, t, z) - f_\theta(x_t, t, z)\|^2}{2\sigma_t^2} \right] \end{aligned} \quad (18)$$

So another weaker upper bound is given by

$$\begin{aligned} & \mathbb{E}_{p(z)} \mathbb{E}_{p_{\text{pre}}(x_0|z)} [-(r(x_0, z) + \gamma) \log p_\theta(x_0|z)] \\ & \leq \mathbb{E}_{p(z)} \mathbb{E}_{p_{\text{pre}}(x_0|z)} [\mathbb{E}_{q(x_T|x_0, z)} [(r(x_0, z) + \gamma) \text{KL}(q(x_T|x_0) \| p(x_T))] \\ & + \sum_{t>1} \mathbb{E}_{q(x_t|x_0, z)} \left[\frac{r(x_0, z) \|x_0 - f_\theta(x_t, t, z)\|^2}{2\sigma_t^2} \right. \\ & \left. + \frac{\gamma (\|x_0 - f_{\text{pre}}(x_t, t, z)\|^2 + \|f_{\text{pre}}(x_t, t, z) - f_\theta(x_t, t, z)\|^2)}{2\sigma_t^2} \right] \\ & - \mathbb{E}_{q(x_1|x_0, z)} [(r(x_0, z) + \gamma) \log p_\theta(x_0|z, x_1)]. \end{aligned} \quad (19)$$

Notice that $p_\theta(x_0|z, x_1)$ is modeled as a discrete decoder as in [10] and $p(x_T|z)$ is a fixed Gaussian; neither is trainable. Then the proof is complete.

B Experimental Details

Online RL training. For hyper-parameters of online RL training used in Section 5.2., we use $\alpha = 10$, $\beta = 0.01$, learning rate = 10^{-5} and keep other default hyper-parameters in AdamW, sampling batch size $m = 10$. For policy gradient training, to perform more gradient steps without the need of re-sampling, we perform 5 gradient steps per sampling step, with gradient norm clipped to be smaller than 0.1, and use importance sampling to handle off-policy samples, and use batch size $n = 32$ in each gradient step. We train the models till it generates 20000 online samples, which matches the number of samples in supervised fine-tuning and results in 10K gradient steps in total. For stable training, we freeze the weights in batch norm to be exactly the same as the pretrained diffusion model. We also explore the use of the ‘‘baseline function’’ to reduce the variance during gradient estimation: we fit a value function $V(x_t, t, z)$ to estimate the expected reward of x_0 using the current policy. In practice, we find that such value function helps to achieve faster training under the single-prompt setting, but would cause instability in training under the multi-prompt setting. We expect the instability comes from not having enough samples to fit the value function, making the gradient estimation biased and thus causing failure in training. We plan to explore the use of a value function under the multi-prompt setting as future work.

Supervised training. For hyper-parameters of supervised training, we use $\gamma = 2.0$ as the default option in Section 5.2, which is chosen from $\gamma \in \{0.1, 1.0, 2.0, 5.0\}$. We use learning rate = 2×10^{-5} and keep other default hyper-parameters in AdamW, which was chosen from $\{5 \times 10^{-6}, 1 \times 10^{-5}, 2 \times 10^{-5}, 5 \times 10^{-5}\}$. We use batch size $n = 128$ and $M = 20000$ such that both algorithms use the same number of samples, and train the SFT model for 8K gradient steps. Notice that Lemma 4.3 requires $r + \gamma$ to be non-negative, we apply a filter of reward such that if $r + \gamma < 0$, we just set it to 0. In practice, we also observe that without this filtering, supervised fine-tuning could fail during training, which indicates that our assumption is indeed necessary.

C Investigation on ImageReward

We investigate the quality of ImageReward [43] by evaluating its prediction of the assessments of human labelers. Similar to Lee et al. [18], we check whether ImageReward generates a higher score for images preferred by humans. Our evaluation encompasses four text prompt categories: color, count, location, and composition. To generate prompts, we combine words or phrases from each category with various objects. These prompts are then used to generate corresponding images using a pre-trained text-to-image model. We collect binary feedback from human labelers on the image-text dataset and construct comparison pairs based on this feedback. Specifically, we utilize 804, 691, 1154 and 13228 comparison pairs obtained from 38, 29, 41 and 295 prompts for color, location, count, and composition, respectively.³ Additionally, for evaluation on complex text prompts from human users, we also utilize the test set from ImageReward, which consists of 6399 comparison pairs from 466 prompts.⁴ Table 2 compares the accuracy of ImageReward and baselines like CLIP [28] and BLIP [19] scores, which justifies the choice of using ImageReward for fine-tuning text-to-image models.

	Color	Count	Location	Composition	Complex
CLIP	82.46	66.11	80.60	70.98	54.83
BLIP	77.36	61.61	78.14	70.98	57.79
ImageReward	86.06	73.65	79.73	79.65	65.13

Table 2: Accuracy (%) of CLIP score, BLIP score and ImageReward when predicting the assessments of human labelers.

D A Comprehensive Discussion of Related Work

We summarize several similarities and differences between our work and a concurrent work [2] as follows:

- Both Black et al. [2] and our work explored online RL fine-tuning for improving text-to-image diffusion models. However, in our work, we provide theoretical insights for optimizing the reward with policy gradient methods and provide conditions for the equivalence to hold.
- Black et al. [2] demonstrated that RL fine-tuning can outperform supervised fine-tuning with reward-weighted loss [18] in optimizing the reward, which aligns with our own observations.
- In our work, we do not only focus on reward optimization: inspired by failure cases (e.g., over-saturated or non-photorealistic images) in supervised fine-tuning [18], we aim at finding an RL solution with KL regularization to solve the problem.
- Unique to our work, we systematically analyze KL regularization for both supervised and online fine-tuning with theoretical justifications. We show that KL regularization would be more effective in the online RL fine-tuning rather than the supervised fine-tuning. By adopting online KL regularization, our algorithm successfully achieves high rewards and maintains image quality without over-optimization issue.

E More Experimental Results

E.1 Multi-prompt Training

Here we report more details for multi-prompt training. We still use the learning rate 10^{-5} as the single prompt setting, but increase the batch size per sampling step to $n = 45$ for stable training. Also, we train for a longer time for multi-prompt such that it utilizes 50000 online samples.

³Full list of text prompts is available at [link].

⁴<https://github.com/THUDM/ImageReward/blob/main/data/test.json>

E.2 Long and Complex Prompts

We show that our method does not just work for short and simple prompts like "A green colored rabbit", but can also work with long and complex prompts. For example, in Fig. 8 we adopt a complex prompt and compare the images generated by the original model and the supervised fine-tuned model. We can observe that online training encourages the models to generate images with a different style of painting and more fine-grained details, which is generally hard to achieve by supervised fine-tuning only (with KL-O regularization, $\gamma = 2.0$).

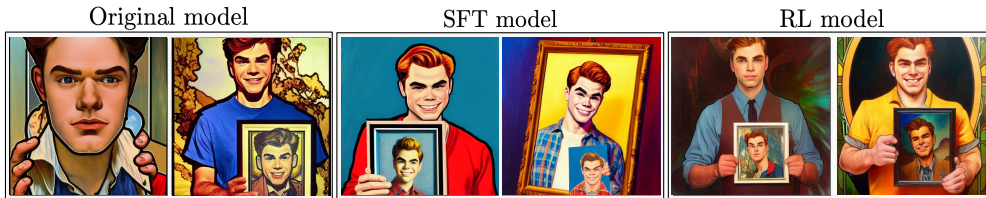


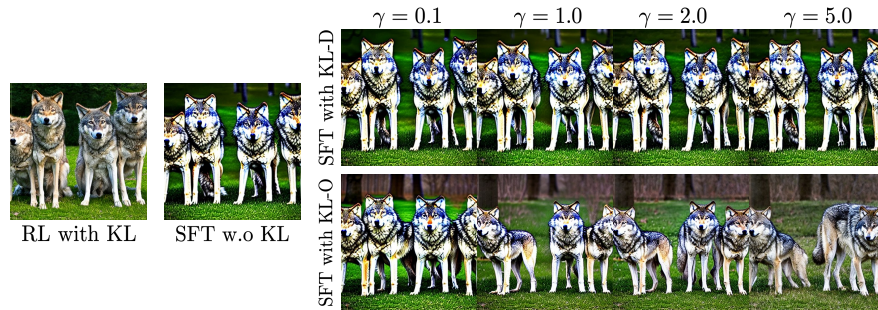
Figure 8: Text prompt: "oil portrait of archie andrews holding a picture of among us, intricate, elegant, highly detailed, lighting, painting, artstation, smooth, illustration, art by greg rutowski and alphonse mucha".

E.3 More Qualitative Results from Ablation Study for KL Regularization in SFT

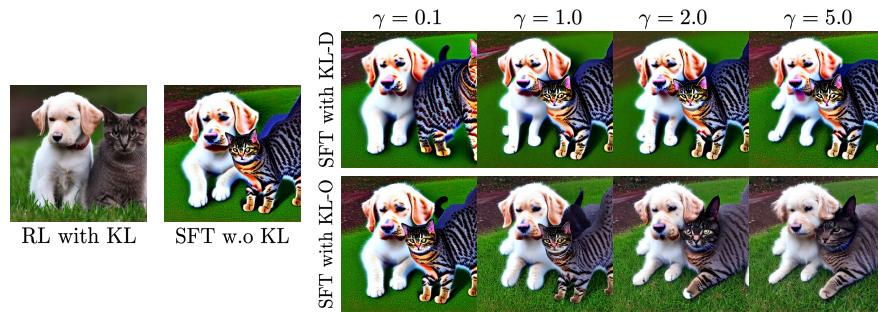
Here we provide samples from more prompts in KL ablation for SFT: see Figure 9.

E.4 Qualitative Comparison

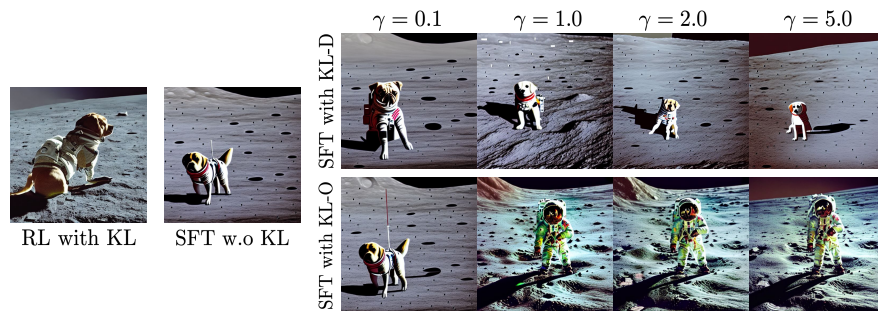
Here we provide more samples from the experiments in Section 5.2 and Section 5.3: see Figure 10, Figure 12, Figure 11, Figure 13, Figure 14 and Figure 15, with the same configuration as in Section 5.2 for both RL and SFT.



(a) "Four wolves in the park"

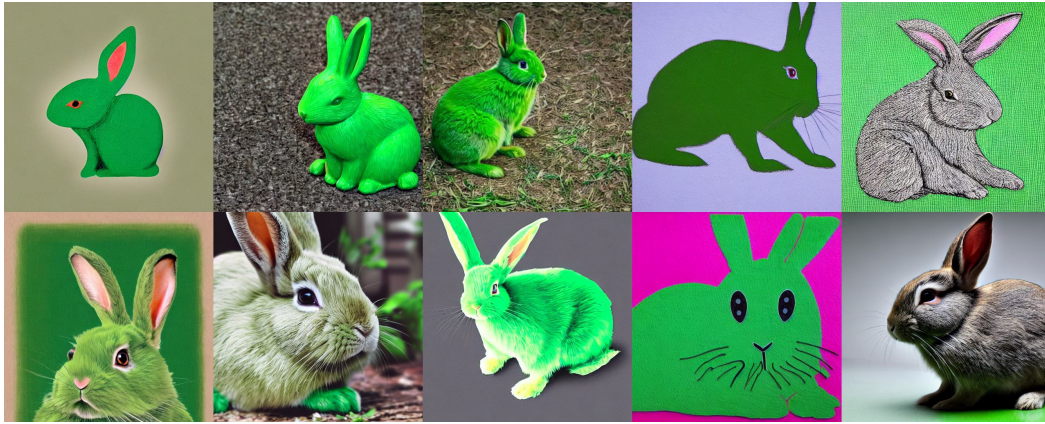


(b) "A cat and a dog"

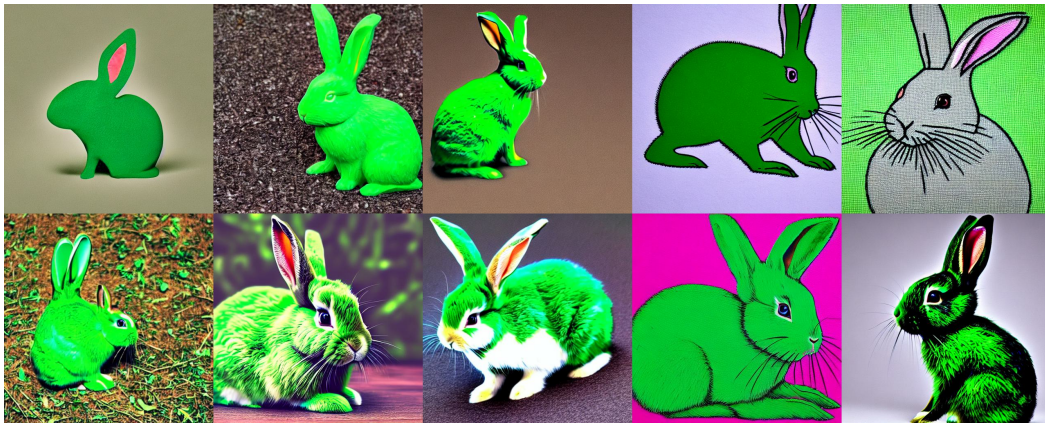


(c) "A dog on the moon"

Figure 9: Samples from supervised fine-tuned models with different KL regularization and KL coefficients.



(a) Original model



(b) SFT model



(c) RL model

Figure 10: Randomly generated samples from (a) the original Stable Diffusion model, (b) supervised fine-tuned (SFT) model and (c) RL fine-tuned model.



(a) Original model



(b) SFT model



(c) RL model

Figure 11: Randomly generated samples from (a) the original Stable Diffusion model, (b) supervised fine-tuned (SFT) model and (c) RL fine-tuned model.



(a) Original model

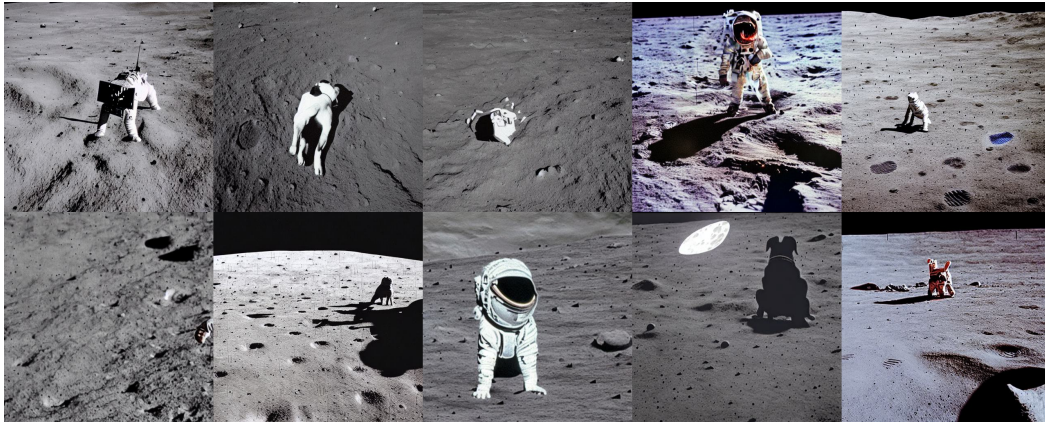


(b) SFT model

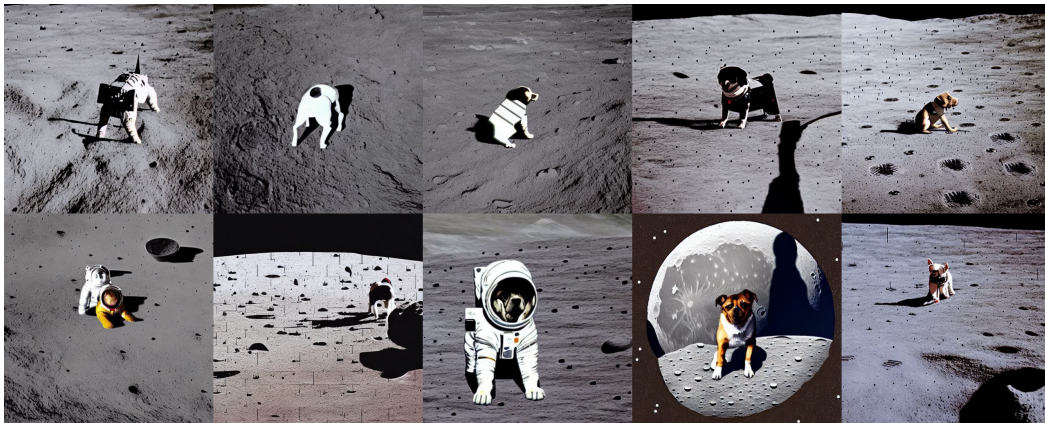


(c) RL model

Figure 12: Randomly generated samples from (a) the original Stable Diffusion model, (b) supervised fine-tuned (SFT) model and (c) RL fine-tuned model.



(a) Original model



(b) SFT model



(c) RL model

Figure 13: Randomly generated samples from (a) the original Stable Diffusion model, (b) supervised fine-tuned (SFT) model and (c) RL fine-tuned model.



(a) RL model without KL regularization

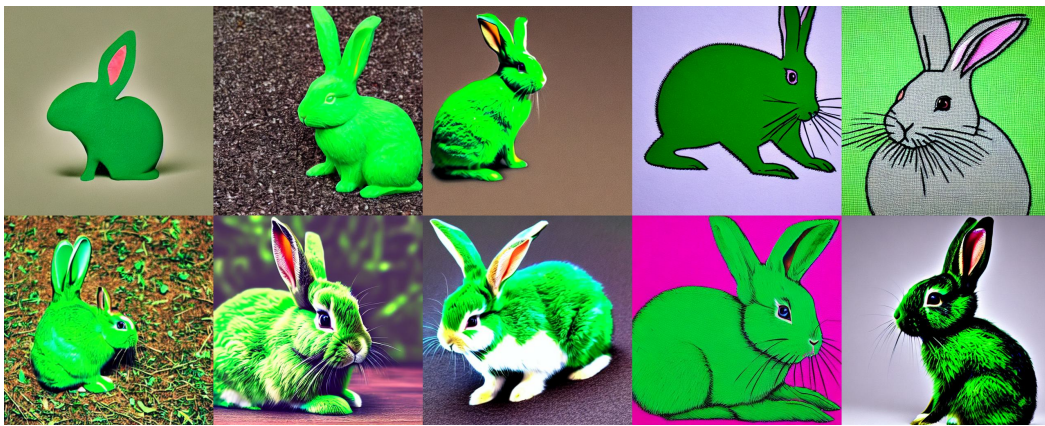


(b) RL model with KL regularization

Figure 14: Randomly generated samples from RL fine-tuned models (a) without and (b) with KL regularization.



(a) SFT model without KL regularization



(b) SFT model with KL regularization

Figure 15: Randomly generated samples from supervised fine-tuned (SFT) models (a) without and (b) with KL regularization.